ISSN 1 746-7233, England, UK
World Journal of Modelling and Simulation
Vol. 8 (2012) No. 3, pp. 205-210

Filter design using multi-bragg reflectors

Fairuz Diyana Ismail[1]*, Muhammad Safwan Aziz[1], Chat Teeka[2], Jalil Ali[1], Preecha Phromphan Yupapin[3]

[1] nstitute of Advanced Photonics Science, Nanotechnology Research Alliance Universiti Teknologi Malaysia (UTM), Johor Bahru 81310, Malaysia

[2] Scientific Equipment Center, Faculty of Science and Technology Suan Dusit Rajabhat University, Bangkok 10700, Thailand

[3] Nanoscale Science and Engineering Research Alliance, Faculty of Science King Mongkut's Institute of Technology Ladkrabang, Bangkok 10520, Thailand

(*Received February 9 2011, Accepted December 8 2011*)

Abstract. In this paper, we present the use of mathematical modeling of dielectric mirror known as known as a Bragg reflector for optical design. A device system consists of the identical alternating layers using high and low refractive indices. Results obtained have shown that the model applications such as quarter-wavelength layers, unequal-length layers, short-pass and long-pass filters, and transmission filter design can be simulated and plotted.

Keywords: dielectric mirror; bragg reflector, quarter-wavelength layers, Fabry-Perot resonator (FPR)

1 Introduction

Higher-order transfer functions can be used to achieve the broader reflectionless notches and in the design of thin-film antireflection coatings, dielectric mirrors, and optical interference filters[1, 4, 6, 8], and in the design of broadband terminations of transmission lines. They are also used in the analysis, synthesis, and simulation of fiber Bragg gratings[7, 9, 10], in the design of narrow-band transmission filters for wavelength-division multiplexing (WDM), and in other fiber-optic signal processing systems[3]. They are routinely used in making acoustic tube models for the analysis and synthesis of speech, with the layer recursions being mathematically equivalent to the Levinson lattice recursions of linear prediction. The layer recursions are also used in speech recognition, disguised as the Schur algorithm. In this paper, we proposed the mathematical modeling of nine-layer dielectric mirrors, it is known as a Bragg reflector. The main interest in dielectric mirrors is that they have extremely low losses at optical and infrared frequencies, as compared to ordinary metallic mirrors, which can be useful for widely optical device applications.

2 Theory

A dielectric mirror (a Bragg reflector) consists of high and low refractive indices, as shown in Fig. 1. The optical thicknesses are typically chosen to be quarter-wavelength long, that is, $n_H l_H = n_L l_L = \lambda/4$ at some operating wavelength λ. The standard arrangement is to have an odd number of layers, with the high index layer being the first and last layer. Fig. 1 shows the case of nine layers. If the number of layers is $M = 2N + 1$, the number of interfaces will be $2N + 2$ and the number of media $2N + 3$. After the first layer, we may view the structure as the repetition of N identical bilayers of low and high indices. The elementary reflection coefficients having the alternative sign as shown in Fig. 1 and are given by

* Corresponding author. *E-mail address*: kypreech@kmitl.ac.th.

$$\rho = \frac{n_H - n_L}{n_H + n_L}, \quad -\rho = \frac{n_L - n_H}{n_L + n_H}, \quad \rho_1 = \frac{n_a - n_H}{n_a + n_H}, \quad \rho_2 = \frac{n_H - n_b}{n_H + n_b}, \tag{1}$$

where n_H, n_L, n_a, and n_b are refractive indices for high, low, air and substrate layers, respectively. The substrate n_b can be arbitrary, even the same as the incident medium n_a. In that case, $\rho_2 = -\rho_1$. The reflectivity properties of the structure can be understood by propagating the impedances from bilayer to bilayer. For the example of Fig. 1, we have for the quarter-wavelength case:

$$Z_2 = \frac{\eta_L^2}{Z_3} = \frac{\eta_L^2}{\eta_H^2} Z_4 = \left(\frac{n_H}{n_L}\right)^2 Z_4 = \left(\frac{n_H}{n_L}\right)^4 Z_6 = \left(\frac{n_H}{n_L}\right)^6 Z_8 = \left(\frac{n_H}{n_L}\right)^8 \eta_b.$$

Therefore, after each bilayer, the impedance decreases by a factor of $(n_L/n_H)^2$. After N bilayers, we will have

$$Z_2 = \left(\frac{n_H}{n_L}\right)^{2N} \eta_b. \tag{2}$$

Using $Z_1 = \eta_H^2/Z_2$, the reflection response at λ_{0is} given by

$$\Gamma_1 = \frac{Z_1 - \eta_a}{Z_1 + \eta_a} = \frac{1 - \left(\frac{n_H}{n_L}\right)^{2N} \frac{n_H^2}{n_a n_b}}{1 + \left(\frac{n_H}{n_L}\right)^{2N} \frac{n_H^2}{n_a n_b}}.$$

It follows that for large N, Γ_1 will tend to -1, that is, 100 % reflection. For nine layers, $2N + 1 = 9$, or $N = 4$, and $n_H = 232$, $n_L = 138$, and $n_a = n_b = 1$, we find: $|\Gamma_1|^2 = 98.84\%$

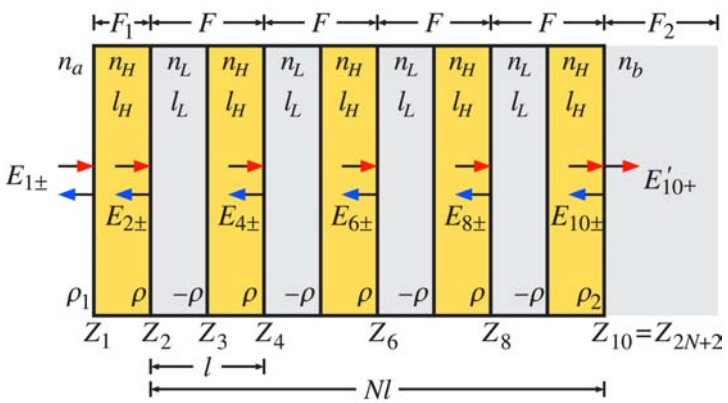

Fig. 1. Nine-layer dielectric mirror

By using the layer recursions, the bandwidth around λ_0 for which the structure exhibits high reflectivity can be determined. Because the bilayers are identical, the forward/backward fields at the left of one bilayer are related to those at the left of the next one by a transition matrix F, which is the product of two propagation matrices of the type of Eq. (2). The repeated application of the matrix F takes us to the right-most layer. For example, in Fig. 1 we have

$$\begin{bmatrix} E_{2+} \\ E_{2-} \end{bmatrix} = F \begin{bmatrix} E_{4+} \\ E_{4-} \end{bmatrix} = F^2 \begin{bmatrix} E_{6+} \\ E_{6-} \end{bmatrix} = F^3 \begin{bmatrix} E_{8+} \\ E_{8-} \end{bmatrix} = F^4 \begin{bmatrix} E_{10+} \\ E_{10-} \end{bmatrix},$$

where F is the matrix:

$$F = \frac{1}{1+\rho} \begin{bmatrix} e^{jk_L l_L} & \rho e^{-jk_L l_L} \\ \rho e^{jk_L l_L} & e^{-jk_L l_L} \end{bmatrix} \frac{1}{1-\rho} \begin{bmatrix} e^{jk_H l_H} & -\rho e^{-jk_H l_H} \\ -\rho e^{jk_H l_H} & e^{-jk_H l_H} \end{bmatrix}.$$

Defining the phase thicknesses $\delta_H = k_H l_H$ and $\delta_L = k_L l_L$, and multiplying the matrix factors out, we obtain the expression for F by

$$F = \frac{1}{1-\rho^2}\begin{bmatrix} e^{j(\delta_H+\delta_L)} - \rho^2 e^{j(\delta_H-\delta_L)} & -2j\rho e^{-j\delta_H}\sin\delta_L \\ 2j\rho e^{j\delta_H}\sin\delta_L & e^{-j(\delta_H+\delta_L)} - \rho^2 e^{-j(\delta_H-\delta_L)} \end{bmatrix}.$$

By an additional transition matrix F_1, we can get to the left of interface-1 and by an additional matching matrix F_2, we can pass to the right of the last interfacing layer.

$$\begin{bmatrix} E_{1+} \\ E_{1-} \end{bmatrix} = F_1 \begin{bmatrix} E_{2+} \\ E_{2-} \end{bmatrix} = F_1 F^4 \begin{bmatrix} E_{10+} \\ E_{10-} \end{bmatrix} = F_1 F_2 F^4 \begin{bmatrix} E_{8+} \\ E_{8-} \end{bmatrix} = F^4 \begin{bmatrix} E'_{10+} \\ 0 \end{bmatrix},$$

where F_1 and F_2 are given by

$$F_1 = \frac{1}{\tau_1}\begin{bmatrix} e^{jk_H l_H} & \rho_1 e^{-jk_H l_H} \\ \rho_1 e^{jk_H l_H} & e^{-jk_H l_H} \end{bmatrix}, \quad F_2 = \frac{1}{\tau_2}\begin{bmatrix} 1 & \rho_2 \\ \rho_2 & 1 \end{bmatrix}, \tag{3}$$

where $\tau_1 = 1+\rho_1$, $\tau_2 = 1+\rho_2$, and ρ_1, ρ_2 were defined in Eq. (1). More generally, for $2N+1$ layers, or N bilayers, we have

$$\begin{bmatrix} E_{2+} \\ E_{2-} \end{bmatrix} = F^N \begin{bmatrix} E_{2N+2,+} \\ E_{2N+2,-} \end{bmatrix}, \quad \begin{bmatrix} E_{1+} \\ E_{1-} \end{bmatrix} = F_1 F_2 F^N \begin{bmatrix} E'_{2N+2,+} \\ 0 \end{bmatrix}.$$

Thus, the properties of the multilayer structure are essentially determined by the N^{th} power, F^N, of the bilayer transition matrix F. In turn, the behavior of F^N is determined by the eigenvalue structure of F.

The eigenvalues $\lambda\pm$ can be both either real or complex values with a unit magnitude. We can represent them in the equivalent form as

$$\lambda_+ = e^{jKl},\ \lambda_- = e^{-jKl},$$

where l is the length of each bilayer, $l = l_L + l_H$. The quantity K is referred to as the Bloch wave-number. If the eigenvalues $\lambda_\pm$ are unit magnitude complex values, then$K$ is real. If the eigenvalues are real values, then K is pure imaginary, say $K = -j\alpha$, so that $\lambda_\pm = e^{\pm jKl} = e^{\pm\alpha l}$.

The eigenvalues are determined from the characteristic polynomial of F, given by the following expression which is valid for any 2×2 matrix as

$$\det(F - \lambda I) = \lambda^2 - (trF)\,\lambda + \det F,$$

where I is the 2×2 identity matrix. The solutions for the left and right bandedges and the bandwidth in λ are given by

$$\lambda_1 = \frac{\pi(n_H l_H + n_L l_L)}{a\cos(-\rho)}, \quad \lambda_2 = \frac{\pi(n_H l_H + n_L l_L)}{a\cos(\rho)}, \quad \Delta\lambda = \lambda_2 - \lambda_1. \tag{4}$$

Similarly, the left/right bandedges in frequency are $f_1 = c/\lambda_2$ and $f_2 = c/\lambda_1$ as given by

$$f_1 = c_0\frac{a\cos(\rho)}{\pi(n_H l_H + n_L l_L)}, \quad f_2 = c_0\frac{a\cos(-\rho)}{\pi(n_H l_H + n_L l_L)}.$$

Noting that $a\cos(-\rho) = \pi/2 + a\sin(\rho)$ and $a\cos(\rho) = \pi/2 - asin(\rho)$, the frequency bandwidth can be written in the equivalent forms as

$$\Delta f = f_2 - f_1 = c_0\frac{a\cos(-\rho) - a\cos(\rho)}{\pi(n_H l_H + n_L l_L)} = c_0\frac{2a\sin(\rho)}{\pi(n_H l_H + n_L l_L)}.$$

Relative to some desired wavelength $\lambda = c/f$, the normalized bandwidths in wavelength and frequency are given by

$$\frac{\Delta\lambda}{\lambda_0} = \frac{\pi\left(n_H l_H + n_L l_L\right)}{\lambda_0}\left[\frac{1}{a\cos\left(\rho\right)} - \frac{1}{a\cos\left(-\rho\right)}\right], \tag{5}$$

$$\frac{\Delta f}{f_0} = \frac{2\lambda_0 a\sin\left(\rho\right)}{\pi\left(n_H l_H + n_L l_L\right)}. \tag{6}$$

Similarly, the center of the reflecting band $f_c = (f_1 + f_2)/2$ is given by

$$\frac{f_c}{f_0} = \frac{\lambda_0}{2\left(n_H l_H + n_L l_L\right)}.$$

If the layers have equal quarter-wave optical lengths at $\lambda 0$, that is, $n_H l_H = n_L l_L = \lambda_0/4$, then, $f_c = f_0$ and the matrix F takes the simplified form as

$$F = \frac{1}{1-\rho^2}\begin{bmatrix} e^{2j\delta} - \rho^2 & -2j\rho e^{-j\delta}\sin\delta \\ 2j\rho e^{j\delta}\sin\delta & e^{-2j\delta} - \rho^2 \end{bmatrix},$$

where $\delta = \delta_H = \delta_L = 2\pi(n_H l_H)/\lambda = 2\pi(\lambda_0/4)/\lambda = (\pi/2)\lambda_0/\lambda = \pi/2)f/f_0$. Then, Eqs. (5) and (6) are simplified into the form as

$$\frac{\Delta\lambda}{\lambda_0} = \frac{\pi}{2}\left[\frac{1}{a\cos\left(\rho\right)} - \frac{1}{a\cos\left(-\rho\right)}\right], \quad \frac{\Delta f}{f_0} = \frac{4}{\pi}a\sin\left(\rho\right). \tag{7}$$

3 Simulation results

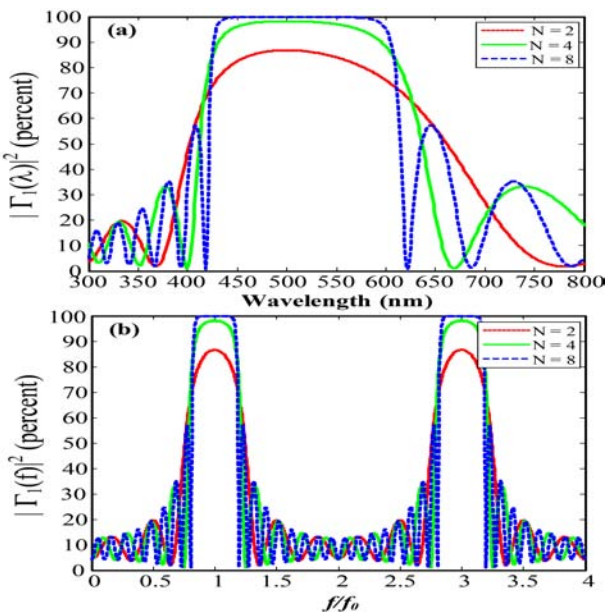

Fig. 2. Dielectric mirror with quarter-wavelength layers

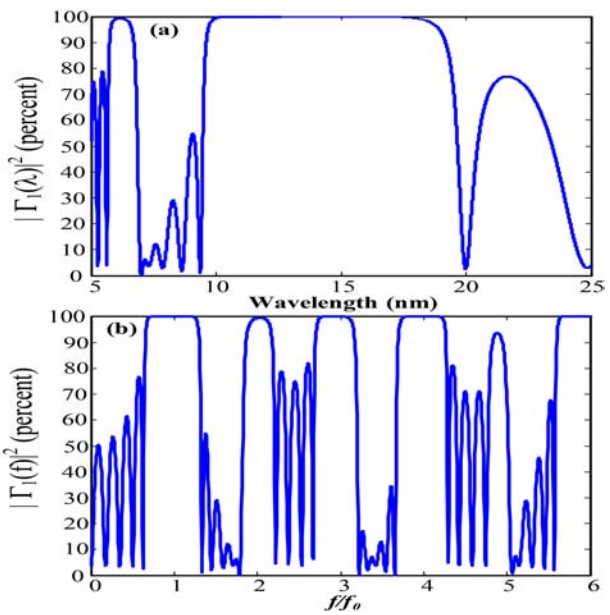

Fig. 3. Shows the reflection response of a mirror having unequal optical lengths for the high and low index films

3.1 Dielectric mirror with quarter-wavelength layers

Fig. 2 shows the reflection response $|\Gamma_1|^2$ as a function of the free-space wavelength λ and as a function of frequency $f = c/\lambda$. The high and low indices are $n_H = 232$ and $n_L = 138$, corresponding to zinc sulfide (ZnS) and magnesium fluoride. The incident medium is air and the substrate is glass with indices $n_a = 1$ and

$n_b = 152$. In Fig. 2(a) depicts the response for the cases of $N = 2, 4, 8$ bilayers, or $2N + 1 = 5, 9, 17$ layers, as defined in Fig. 1. The design wavelength at which the layers are quarter-wavelength long is $\lambda = 500nm$. The reflection coefficient is $\rho = 0.25$ and the ratio $n_H/n_L = 168$. The wavelength bandwidth calculated from Eq. (7) is $\Delta\lambda = 16802nm$ and has been placed on the graph at an arbitrary reflectance level. The left/right bandedges are $\lambda_1 = 42973, \lambda_2 = 59775nm$. The bandwidth covers most of the visible spectrum. As the number of bilayers N increases, the reflection response becomes flatter within the bandwidth $\Delta\lambda$, and has sharper edges and tends to 100%. The bandwidth $\Delta\lambda$ represents the asymptotic width of the reflecting band.

In Fig. 2(b) depicts the reflection response as a function of frequency f and is plotted in the normalized variable f/f. Because the phase thickness of each layer is $\delta = \pi f/2f$ and the matrix F is periodic in δ, the mirror behavior of the structure will occur at odd multiples of f (or odd multiples of $\pi/2$ for δ.), the structure acts as a sampled system with sampling frequency $f_s = 2f$, and therefore, $f = f_s/2$ plays the role of the Nyquist frequency.

The frequency graph shows only the case of $N = 8$. The bandwidth Δf, calculated from Eq. (7), has been placed on the graph. The maximum reflectance (evaluated at odd multiples of f) is equal to 99.97%.

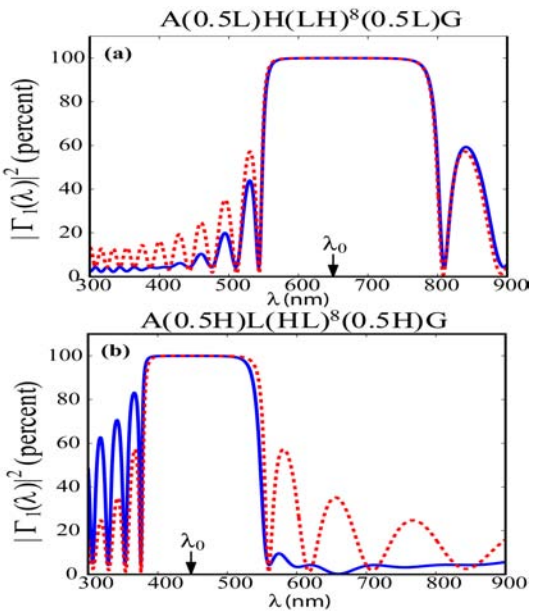

Fig. 4. Short- and long-pass wavelength filters

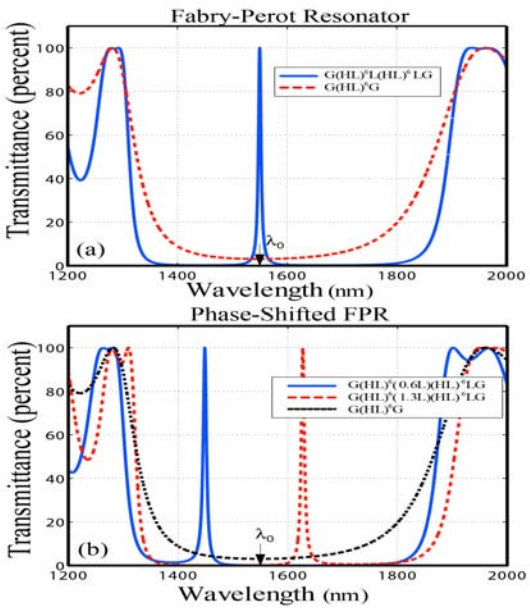

Fig. 5. Narrowband FPR transmission filters

3.2 Dielectric mirror with unequal-length layers

The reflection response of a mirror having unequal optical lengths for the high and low index films is as shown in Fig. 3. The parameters of this example correspond very closely to the recently constructed omnidirectional dielectric mirror[2, 5], which was designed to be a mirror over the infrared band of 10–15μm. The number of layers is nine and the number of bilayers, $N = 4$. The indices of refraction are $n_H = 46$ and $n_L = 16$ corresponding to Tellurium and Polystyrene. Their ratio is $n_H/n_L = 2.875$ and the reflection coefficient, $\rho = 0.48$. The incident medium and substrate are air and NaCl ($n = 1.48$), in which the center wavelength is taken to be at the middle of the 10–15μm band, that is, $\lambda = 12.5\mu m$. The lengths of the layers are $l_H = 0.8$ and $l_L = 1.65\mu m$, resulting in the optical lengths (relative to λ) $n_H l_H = 0.2944\lambda$ and $n_L l_L = 0.2112\lambda$. The wavelength bandwidth, calculated from Eq. (5), is $\Delta\lambda = 9.07\mu m$.

3.3 Short-pass and long-pass filters

By adding an eighth-wave low-index layer, that is, a $(0.5L)$, at both ends are the same as in previous section, we can decrease the reflectivity of the short wavelengths. Thus, the stack $AH(LH)^8G$ is replaced

by $A(0.5L)H(LH)^8(0.5L)G$. For example, suppose we wish to have high reflectivity over the [600, 700] nm range and low reflectivity below 500 nm. In Fig. 4(a) shows the resulting reflectance with the design wavelength chosen to be $\lambda_0 = 650nm$. The parameters n_a, n_b, n_H, n_L are the same as in previous section. In Fig. 4(b) shows the stack $A(0.5H)L(HL)^8(0.5H)G$ obtained from the previous case by interchanging the roles of H and L. Now, the resulting reflectance is low for the higher wavelengths. The design wavelength was chosen to be $\lambda_0 = 450nm$. It can be seen from the graph that the reflectance is high within the band [400, 500] nm and low above 600 nm.

3.4 Transmission filter design with one Fabry-Perot resonator (FPR)

This example illustrates the basic transmission properties of FPR filters. We choose parameters that might closely emulate the case of a fiber Bragg grating for WDM applications. The refractive indices of the left and right substrates and the layers were: $n_a = n_b = 152, n_L = 14$, and $n_H = 21$. The design wavelength at which the layers are quarter wavelength is taken to be the standard laser source $\lambda = 1550nm$. First, we compare the cases of a dielectric mirror $(HL)^N$ and its phase-shifted version using a single FPR (cases 0 and 1 in Eq. (1)), with number of layers $N_1 = 6$. Fig. 5 shows the transmittance, that is, the quantity $(1|\Gamma_1(\lambda)|^2)$ plotted over the range $1200 \leq \lambda \leq 2000$ nm. We observe that the mirror (case 0) has a suppressed transmittance over the entire reflecting band, whereas the FPR filter (case 1) has a narrow peak at λ. The asymptotic edges of the reflecting band are calculated from Eq. (4) to be $\lambda_1 = 1373.9nm$ and $\lambda_2 = 1777.9nm$, resulting in a width of $\Delta\lambda = 404nm$.

4 Conclusion

Mathematical modeling of dielectric mirror consists of identical alternating layers of high and low refractive indices are presented. Simulation results of the applications such as quarter-wavelength layers, unequal-length layers, short-pass and long-pass filters, and transmission filter design are obtained and plotted, which is shown that the location of the output peak can be shifted by making the phase-shift different from $\lambda/4$. This can be accomplished by changing the optical thickness of the middle L-layer to some other value.

References

[1] D. Chigrin, A. Lavrinenko, et al. Observation of total omnidirectional reflection from a one-dimensional dielectric lattice. *Journal of Applied Physics*, 1999, **68**(A): 25.

[2] D. Chigrin, A. Lavrinenko, et al. Observation of total omnidirectional reflection from a one-dimensional dielectric lattice. *Journal of Applied Physics A*, 1999, **68**: 25.

[3] E. Dowling, D. MacFarlane. Lightwave lattice filters for optically multiplexed communication systems. *Journal of Lightwave Technology*, 1994, **12**: 471.

[4] Y. Fink, D. Ripin, et al. Guiding optical light in air using an all-dielectric structure. *Journal of Lightwave Technology*, 1999, **17**: 2039.

[5] Y. Fink, J. Winn, et al. A dielectric omnidirectional reflector. *Science*, 1998, **282**: 1679.

[6] L. Li, J. Dobrowolski. High-performance thin-film polarizing beam splitter operating at angles greater than the critical angle. *Applied Optics*, 2000, **39**: 2754.

[7] S. Nafisah, H. Hairi, et al. Novel design of multiplexed sensors using a dual fbgs scheme. *Microwave and Optical Technology Letters*, 2010, **52**(5): 1218–1221.

[8] K. Popov, J. Dobrowolski, et al. Broadband high-reflection multilayer coatings at oblique angles of incidence. *Applied Optics*, 1997, **36**: 2139.

[9] T. Saktioto, H. Hairi, et al. Nonlinear parametric studies of photon in a fiber bragg grating. **in:** *2009 IEEE Symposium on Industrial Electronics and Applications, ISIEA 2009—Proceedings 1*, 2009, 355–357.

[10] T. Saktioto, H. Hairi, et al. Nonlinear parametric study of photon in a fibre bragg grating. *Physics Procedia*, 2009, **2**(1): 81–85.